REPORT DOCUMENTATION PAGE

Form Approved OMB NO. 0704-0188

1. REPORT DATE (DD-MM-YYYY)	2. REPORT TYPE	3. DATES COVERED (From - To)
12-12-2008	New Reprint	4-Mar-2007 - 2-Jul-2008

4. TITLE AND SUBTITLE
Time-dependent stochastic inversion in acoustic tomography of the atmosphere with reciprocal sound transmission

5a. CONTRACT NUMBER
W911NF-06-1-0007

5b. GRANT NUMBER

5c. PROGRAM ELEMENT NUMBER
206022

6. AUTHORS
S. N. Vecherin, D. K. Wilson, V. E. Ostashev, A. Zieman

5d. PROJECT NUMBER

5e. TASK NUMBER

5f. WORK UNIT NUMBER

7. PERFORMING ORGANIZATION NAMES AND ADDRESSES
New Mexico State University
1620 Standley Drive
Academic Research Bldg A, Room 110
Las Cruces, NM 88003 -

8. PERFORMING ORGANIZATION REPORT NUMBER

9. SPONSORING/MONITORING AGENCY NAME(S) AND ADDRESS(ES)
U.S. Army Research Office
P.O. Box 12211
Research Triangle Park, NC 27709-2211

10. SPONSOR/MONITOR'S ACRONYM(S)
ARO

11. SPONSOR/MONITOR'S REPORT NUMBER(S)
49504-EV-HSI.10

12. DISTRIBUTION AVAILIBILITY STATEMENT
Approved for Public Release; Distribution Unlimited

13. SUPPLEMENTARY NOTES
The views, opinions and/or findings contained in this report are those of the author(s) and should not contrued as an official Department of the Army position, policy or decision, unless so designated by other documentation.

14. ABSTRACT
Time-dependent stochastic inversion (TDSI) was recently developed for acoustic travel-time tomography of the atmosphere. This type of tomography allows reconstruction of temperature and wind-velocity fields given the location of sound sources and receivers and the travel times between all source–receiver pairs. The quality of reconstruction provided by TDSI depends on the geometry of the transducer array. However, TDSI has not been studied for the geometry with reciprocal sound transmission. This paper is focused on three aspects of TDSI. First, the use of TDSI in reciprocal sound transmission arrays is studied in numerical and physical experiments. Second, efficiency of time-dependent and ordinary

15. SUBJECT TERMS
acoustic tomography of the atmosphere, temperature and wind velocity fields

16. SECURITY CLASSIFICATION OF:			17. LIMITATION OF ABSTRACT	15. NUMBER OF PAGES	19a. NAME OF RESPONSIBLE PERSON
a. REPORT	b. ABSTRACT	c. THIS PAGE			Vladimir Ostashev
U	U	U	SAR		19b. TELEPHONE NUMBER: 575-646-3831

Report Title

Time-dependent stochastic inversion in acoustic tomography of the atmosphere with reciprocal sound transmission

ABSTRACT

Time-dependent stochastic inversion (TDSI) was recently developed for acoustic travel-time tomography of the atmosphere. This type of tomography allows reconstruction of temperature and wind-velocity fields given the location of sound sources and receivers and the travel times between all source–receiver pairs. The quality of reconstruction provided by TDSI depends on the geometry of the transducer array. However, TDSI has not been studied for the geometry
with reciprocal sound transmission. This paper is focused on three aspects of TDSI. First, the use of TDSI in reciprocal sound transmission arrays is studied in numerical and physical experiments. Second, efficiency of time-dependent and ordinary stochastic inversion (SI) algorithms is studied in numerical experiments. Third, a new model of noise in the input data for TDSI is developed that accounts for systematic errors in transducer positions. It is shown that (i) a separation of the travel times into temperature and wind-velocity components in tomography with reciprocal transmission does not improve the reconstruction, (ii) TDSI yields a better reconstruction than SI and (iii) the developed model of noise yields an accurate reconstruction of turbulent fields and estimation of errors in the reconstruction.

Meas. Sci. Technol. **19** (2008) 125501 (12pp) doi:10.1088/0957-0233/19/12/125501

Time-dependent stochastic inversion in acoustic tomography of the atmosphere with reciprocal sound transmission

Sergey N Vecherin[1,2,5], Vladimir E Ostashev[1,3], D Keith Wilson[2] and A Ziemann[4]

[1] Department of Physics, New Mexico State University, Las Cruces, NM 88003, USA
[2] US Army Engineer Research and Development Center, Hanover, NH 03755, USA
[3] NOAA/Earth System Research Laboratory, Boulder, CO 80305, USA
[4] Institute for Meteorology, University of Leipzig, Stephanstr 3, 04103 Leipzig, Germany

E-mail: Sergey.N.Vecherin@usace.army.mil

Received 14 March 2008, in final form 31 July 2008
Published 17 October 2008
Online at stacks.iop.org/MST/19/125501

Abstract
Time-dependent stochastic inversion (TDSI) was recently developed for acoustic travel-time tomography of the atmosphere. This type of tomography allows reconstruction of temperature and wind-velocity fields given the location of sound sources and receivers and the travel times between all source–receiver pairs. The quality of reconstruction provided by TDSI depends on the geometry of the transducer array. However, TDSI has not been studied for the geometry with reciprocal sound transmission. This paper is focused on three aspects of TDSI. First, the use of TDSI in reciprocal sound transmission arrays is studied in numerical and physical experiments. Second, efficiency of time-dependent and ordinary stochastic inversion (SI) algorithms is studied in numerical experiments. Third, a new model of noise in the input data for TDSI is developed that accounts for systematic errors in transducer positions. It is shown that (i) a separation of the travel times into temperature and wind-velocity components in tomography with reciprocal transmission does not improve the reconstruction, (ii) TDSI yields a better reconstruction than SI and (iii) the developed model of noise yields an accurate reconstruction of turbulent fields and estimation of errors in the reconstruction.

Keywords: travel-time tomography, inverse problems, acoustic imaging, remote sensing, tomography of the atmosphere, stochastic inversion

1. Introduction

Acoustic travel-time tomography of the atmosphere allows one to reconstruct temperature and wind-velocity fields in a certain plane or volume given the coordinates of sound sources and receivers and travel times of sound propagation between all source–receiver pairs [1–6]. In outdoor acoustic tomography experiments [7], the number of sources and receivers has been relatively small (less than 20) so that the number of measured travel times has also been small. Therefore, one of the main issues in acoustic tomography of the atmosphere, similarly to analogous problems in other areas [8–10], is the formulation of robust and accurate inverse algorithms for reconstruction of the temperature and wind-velocity fields from a limited amount of data (the travel times and transducers' coordinates).

To address this issue, a time-dependent stochastic inversion (TDSI) algorithm was recently developed for travel-time tomography of the atmosphere [11–14]. The main idea of TDSI is to measure the travel times repeatedly (i.e., at different times) and to use all these measurements for reconstruction of temperature and wind-velocity fluctuations at an arbitrary moment of time. This can be accomplished by taking into account temporal covariances of the fluctuations. TDSI takes into account both spatial and temporal covariances and, hence, is an improvement over the ordinary stochastic inverse (SI)

[5] Present address: Signature Physics Branch, US Army ERDC-CRREL, 72 Lyme Rd, Hanover, NH 03755-1290, USA.

that accounts for spatial covariances only [1, 15]. For the problem considered in this paper, significant correlations exist in the atmospheric surface layer over time scales of tens of seconds and spatial scales of tens to hundreds of meters. TDSI might also be considered for tomographic applications on a larger scale, such as global atmospheric tomography using infrasound. In this case, it could take advantage of correlations involving synoptic weather patterns, which have correlation time scales of days and spatial scales of hundreds of kilometers.

The general idea of TDSI is successfully applied in other areas. For example, a similar approach is used in satellite altimetry of the ocean surface to interpolate measurements along satellite tracks to other spatial and temporal points [16–18]. In image processing, this approach is used to improve the image quality from several blurred or noisy frames [19, 20]. A similar algorithm is used in medical tomography where it is referred to as the vector Wiener filter [21]. TDSI is also somewhat similar to the Kalman filter [22, 23] which is applied in many areas including tomography [24–27]. The distinction is that TDSI is not recursive (i.e., yields a closed-form reconstruction), does not make assumptions regarding stochastic variables that adopted in Kalman's theory (e.g., does not require formulation of a problem in state-space terms which could be a difficult task) and uses data obtained at arbitrary times for the reconstruction of fluctuations at other arbitrary time (in this paper, for example, the previous, current and future measurements relative to the time of reconstruction are used).

The question about what functions can be used to describe spatial covariances of isotropic, homogeneous and statistically stationary atmospheric turbulence, which is considered in this paper, is well studied in the literature (e.g., [28–32]). The spatial–temporal covariance functions can be obtained from spatial ones with the use of frozen or locally frozen turbulence hypotheses [11, 12, 28]. However, these functions may not coincide with spatial–temporal covariance functions of actual turbulence since (i) the theoretical and actual spatial functions may differ, and (ii) the frozen or locally frozen hypotheses may not describe actual turbulence adequately. As a result, the TDSI algorithm may not yield more accurate reconstruction than an ordinary stochastic inversion algorithm, which utilizes only spatial covariance functions. The advantage of TDSI in comparison with SI was demonstrated in [11] for numerically created rigidly frozen turbulence. However, it has not been shown that TDSI provides a more accurate reconstruction in the case of realistic turbulence which may or may not be frozen.

The goals of the paper are threefold. First, application of TDSI to acoustic tomography with reciprocal sound transmissions is studied. Reciprocal transmission tomographic arrays have been used successfully in underwater and atmospheric tomography for many years [33–36]. There are two advantages of such arrays. First, they allow one to increase the number of measured travel times for a given number of transducer stations since the total number of sound sources and receivers increases. Second, they allow one to separate the originally measured travel times into two components: travel times due to temperature and travel times due to velocity. This makes the contribution of weaker fluctuations to the data apparent. Therefore, one can solve two problems (one for the reconstruction of the temperature field and another one for the reconstruction of the wind-velocity field) more effectively than the original problem, in which temperature and wind-velocity fields are reconstructed simultaneously. However, such a separation reduces the number of travel times for each of the fields by a factor of two. Therefore, the analytical advantage of independent field reconstruction may not lead to better quality. For some algorithms, such an analytical separation led to a better reconstruction (or was a presupposition of some specific algorithms) [6, 36, 37]. However, it has not been studied whether such an approach improves the reconstruction with the use of stochastic algorithms. In this paper, reciprocal transmission arrays are studied for time-dependent and ordinary stochastic inversion algorithms.

The second goal of this paper is to verify that TDSI yields a better reconstruction than SI for realistic turbulence. For this purpose, time-dependent, horizontal slices through temperature and wind-velocity fields from a high-resolution large-eddy simulation (LES) of an unstably stratified atmospheric boundary layer were used as a surrogate atmosphere. The LES solves an approximate, filtered form of the nonlinear fluid dynamic (Navier–Stokes) equations that explicitly describes the large-scale structure of the flow. More detailed information about the LES used in this paper can be found in [38].

Finally, in this paper, a more complete model of noise in the input data for SI and TDSI is developed. This model assumes that the errors (noise) in the transducer positions is systematic; i.e. it remains the same for measurements at different times for a given ray path. Also, the errors in the mean field reconstruction affect data corresponding to all travel paths. These improvements result in a non-diagonal noise matrix, in contrast to earlier publications [11–14].

All derivations are implemented for a two-dimensional problem where all sources and receivers lie in one horizontal plane, and two-dimensional temperature and wind-velocity fields are subject to reconstruction. The derived results remain valid for the three-dimensional case.

The paper is organized as follows. The separation of travel times into temperature and wind-velocity travel times is presented in section 2. The basic equations for the reconstruction of temperature and wind-velocity fields are given in section 3. The numerical experiment with the use of LES fields is described in section 4. Then, application of TDSI to real experimental data from a reciprocal transmission array is demonstrated in section 5. Summary and conclusions are presented in section 6.

2. Separation of travel times

In this section, it is shown how the temperature and wind-velocity contributions to the travel times can be separated. The linearized equation for travel times in two-dimensional acoustic tomography of the atmosphere in the horizontal (x, y)

plane is given by the following equation [11]:

$$t_i^{\mathrm{tr}}(t) = \frac{L_i}{c_0(t)}\left(1 - \frac{u_0(t)s_{ix} + v_0(t)s_{iy}}{c_0(t)}\right) - \frac{1}{c_0^2(t)}\int_{L_i} \mathrm{d}l \left\{\frac{c_0(t)}{2T_0(t)}T(\mathbf{r},t) + u(\mathbf{r},t)s_{ix} + v(\mathbf{r},t)s_{iy}\right\}, \quad (1)$$

where t_i^{tr} is the travel time of a sound propagating along path L_i, $i = 1, 2, \ldots, I$, I being the total number of travel paths (if S is the number of sound sources and R is the number of receivers, then $I = SR$), $\mathbf{V}_0 = u_0\mathbf{e}_x + v_0\mathbf{e}_y$ is the vector of wind velocity spatially averaged over a tomographic plane, $\mathbf{e}_x$ and $\mathbf{e}_y$ are the basis vectors of a Cartesian coordinate system, c_0 and T_0 are adiabatic sound speed and temperature averaged over a tomographic plane, $\mathbf{V} = u\mathbf{e}_x + v\mathbf{e}_y$ and T are fields of fluctuations, $\mathbf{s}_i = s_{ix}\mathbf{e}_x + s_{iy}\mathbf{e}_y$ is a unit vector in the direction of the ith ray propagation, $\mathbf{r} = x\mathbf{e}_x + y\mathbf{e}_y$ is a spatial vector and t is time. The integration is taken along path L_i which, in this approximation, is a straight line. The full fields of temperature and wind velocity in the tomographic plane, $\widetilde{T}(\mathbf{r},t)$ and $\widetilde{\mathbf{V}}(\mathbf{r},t)$, can be found as the sum of their spatial mean values $c_0(t)$ and $\mathbf{V}_0(t)$ and fluctuation fields $T(\mathbf{r},t)$ and $\mathbf{V}(\mathbf{r},t)$:

$$\widetilde{T}(\mathbf{r},t) = T_0(t) + T(\mathbf{r},t), \quad \widetilde{\mathbf{V}}(\mathbf{r},t) = \mathbf{V}_0(t) + \mathbf{V}(\mathbf{r},t). \quad (2)$$

The mean values c_0 and T_0 are connected by the following relationship:

$$c_0^2(t) = \gamma R_a T_0(t), \quad (3)$$

where $\gamma = c_p/c_V \approx 1.41$ is the ratio of specific heats c_p and c_V, and R_a is the gas constant for dry air. Note that $\widetilde{T}$ is the *acoustic virtual* temperature which relates to ordinary thermodynamic temperature T_{th} as $\widetilde{T} = T_{\mathrm{th}}(1 + 0.511C)$, where C is the concentration of water in air [31]. Note that, for small C, $C \cong q$, where q is the specific air humidity. The temporal variations of the mean fields could be significantly greater than the magnitude of the fluctuations. For example, in the field experiment described in [12], T_0 varied from 15.9 to 16.4 °C, u_0 from −0.3 to −1.3 m s^{-1}, and v_0 from −1.6 to −2.1 m s^{-1} during 10 min while the corresponding standard deviations of the fluctuations were $\sigma_T = 0.27$ °C and $\sigma_V = 0.28$ m s^{-1}.

The goal of acoustic travel-time tomography is to reconstruct fields $T_0(t)$, $\mathbf{V}_0(t)$, $T(\mathbf{r},t)$ and $\mathbf{V}(\mathbf{r},t)$ given the coordinates of sound sources and receivers (which determine $\mathbf{s}_i$) and travel times $t_i^{\mathrm{tr}}(t)$ for all rays.

Note that there may exist such wind-velocity fields $\widetilde{\mathbf{V}}$ that are 'invisible' for travel-time tomography in the sense that they do not contribute to the travel times t_i^{tr} [34, 35]. To detect these fields some additional measurements, besides travel times, are suggested [34]. In this paper, no additional measurements are used for reconstruction of wind velocity with the use of stochastic inversion algorithms. The results of such a reconstruction are discussed in section 5.

A reciprocal ray setup provides the travel times for each pair of rays simultaneously propagating in opposite directions. This allows an analytical separation of the measured travel times on two subsets: the travel times t_{iT}^{tr}, which are affected only by $\widetilde{T}$, and travel times t_{iV}^{tr}, which are affected only by $\widetilde{\mathbf{V}}$. Let n and k be indices for reciprocal rays: $n = 1, 2, \ldots, N$, $k = 1, 2, \ldots, N$, and $N = I/2$. Their lengths are the same, $L_n = L_k$, but their directions are opposite: $\mathbf{s}_k = -\mathbf{s}_n$. Taking the sum and difference of the measured travel times t_n^{tr} and t_k^{tr} and using equation (1), one obtains

$$t_{nT}^{\mathrm{tr}}(t) = \frac{t_k^{\mathrm{tr}}(t) + t_n^{\mathrm{tr}}(t)}{2} = \frac{L_n}{c_0(t)} - \frac{1}{2c_0(t)T_0(t)}\int_{L_n} T(\mathbf{r},t)\,\mathrm{d}l, \quad (4)$$

$$t_{nV}^{\mathrm{tr}}(t) = \frac{t_k^{\mathrm{tr}}(t) - t_n^{\mathrm{tr}}(t)}{2} = \frac{L_n(u_0(t)s_{nx} + v_0(t)s_{ny})}{c_0^2(t)} + \frac{1}{c_0^2(t)}\int_{L_n} \mathrm{d}l\,(u(\mathbf{r},t)s_{nx} + v(\mathbf{r},t)s_{ny}). \quad (5)$$

The advantage of equations (4) and (5) in comparison with the original equation (1) is that they allow independent reconstruction of temperature and wind-velocity fields. However, the amount of data for such reconstruction is two times less. Therefore, it is worthwhile comparing the reconstructions based on equation (1) and on equations (4) and (5).

3. Reconstruction of the mean fields

The reconstruction of mean fields $u_0(t)$, $v_0(t)$ and $T_0(t)$ will be based on the same formalism that was utilized in [11–13]. However, the direct application of the formalism, developed in these references, is not possible since the starting equations (i.e., equations (4) and (5)) differ from the original one (equation (1)).

The first step is to neglect fluctuations in equations (4) and (5). This results in omitting the integrals in these equations. Physically, this means that one reconstructs the uniform fields $c_0(t)$ and $\mathbf{V}_0(t)$ which match in the best way the known travel times $t_{nT}^{\mathrm{tr}}(t)$ and $t_{nV}^{\mathrm{tr}}(t)$. The value of T_0 is calculated from c_0 with the use of equation (3). The second step is to use travel times at time t to reconstruct the mean fields at the same time t. Then, time t is a parameter and will be omitted until the end of this section. The fact that travel times depend on t will be used in the following section in which fluctuations $T(\mathbf{r},t)$ and $\mathbf{V}(\mathbf{r},t)$ will be reconstructed by TDSI.

3.1. Reconstruction of mean temperature

After omitting the integral in equation (4), the equation for c_0 can be rewritten in the following form:

$$c_0 = d_{nT}, \quad (6)$$

where $d_{nT} = L_n/t_{nT}^{\mathrm{tr}}$. The well-known least-squares solution $\widehat{c}_0$ and the estimation of its standard deviation $\widehat{\sigma}_{c_0}$ for such a problem are given by the following formulae [15]:

$$\widehat{c}_0 = \frac{\sum_{n=1}^{N} d_{nT}}{N}, \quad (7)$$

$$\widehat{\sigma}_{c_0} = \sqrt{\frac{\sum_{n=1}^{N}(d_{nT} - \widehat{c}_0)^2}{N(N-1)}}. \tag{8}$$

The reconstruction of mean temperature $\widehat{T}_0$ is obtained from $\widehat{c}_0$ with the use of equation (3).

3.2. Reconstruction of mean wind velocity

Once the value of c_0 is reconstructed, one can use equation (5) to reconstruct the mean values of wind-velocity components. Neglecting the fluctuations in equation (5), one can formulate the problem in matrix notation as follows:

$$\mathbf{G}\mathbf{f} = \mathbf{d}_V, \tag{9}$$

where

$$\mathbf{G} = \begin{bmatrix} s_{1x} & s_{1y} \\ \vdots & \vdots \\ s_{Nx} & s_{Ny} \end{bmatrix}, \tag{10}$$

$$\mathbf{f} = [u_0; v_0], \tag{11}$$

and

$$\mathbf{d}_V = c_0^2\left[t_{1V}^{\mathrm{tr}}/L_1; \ldots; t_{NV}^{\mathrm{tr}}/L_N\right]. \tag{12}$$

The semicolon between elements indicates that these elements are arranged in a column so that $\mathbf{f}$ and $\mathbf{d}_V$ are column vectors. In equation (9), the matrix $\mathbf{G}$ and the vector $\mathbf{d}_V$ are known, while the vector $\mathbf{f}$ is subject to estimation. Usually, $N > 2$, and the problem seems to be overdetermined since the number of equations is greater than the number of unknowns. However, the matrix $\mathbf{G}$ could be ill-conditioned due to an unfortunate location of the transmitters and receivers. In this case, the straightforward least-squares solution of equation (9), which implies inversion of matrix $(\mathbf{G}^T\mathbf{G})$, cannot be employed accurately. Therefore, it is worthwhile using the pseudo-inverse [39] matrix $\mathbf{G}_p^{-1}$, in terms of which the solution of equation (9) is given by the following formula:

$$\widehat{\mathbf{f}} = \mathbf{G}_p^{-1}\mathbf{d}_V. \tag{13}$$

If the $\mathbf{G}$ matrix is well conditioned (i.e., its rank equals 2), then $\mathbf{G}_p^{-1}$ coincides with the least-squares estimator: $\mathbf{G}_p^{-1} = (\mathbf{G}^T\mathbf{G})^{-1}\mathbf{G}^T$, and equation (13) yields the least-squares solution of equation (9). If the $\mathbf{G}$ matrix is ill conditioned (i.e., its inverse condition number equals or approaches zero), then it corresponds to the situation when one of the unknowns (u_0 or v_0) is overdetermined while the other is underdetermined. In this case, $\mathbf{G}_p^{-1}$ yields the least-squares solution for the overdetermined unknown and the minimal second norm solution for the underdetermined one.

Similar to equation (8), the mean squared errors $\widehat{\boldsymbol{\sigma}}_{\mathbf{f}}^2 = \left[\widehat{\sigma}_{u_0}^2, \widehat{\sigma}_{v_0}^2\right]$ of the solution $\widehat{\mathbf{f}}$ can be estimated with the help of the residual estimation [12]:

$$\widehat{\boldsymbol{\sigma}}_{\mathbf{f}}^2 = s_{d_V}^2 \operatorname{diag}\left(\mathbf{G}_p^{-1}\left[\mathbf{G}_p^{-1}\right]^T\right), \tag{14}$$

where $s_{d_V}^2$ is the estimated variance in the data $\mathbf{d}_V$:

$$s_{d_V}^2 = \frac{(\mathbf{d}_V - \mathbf{G}\widehat{\mathbf{f}})^T(\mathbf{d}_V - \mathbf{G}\widehat{\mathbf{f}})}{N-2}. \tag{15}$$

The errors $\widehat{\boldsymbol{\sigma}}_{\mathbf{f}}^2$ and $\widehat{\sigma}_{c_0}^2$ take into account the errors in travel time measurements, transducer positions, and omitting the integral term in equations (4) and (5). (Note that errors in travel-time measurements refer to a specific technique of the measurement; they are independent of the errors caused by the transducer position uncertainty or omitting the integral.)

4. Reconstruction of the fluctuations

In this section, the fluctuations $T(\mathbf{r}, t)$ and $\mathbf{V}(\mathbf{r}, t)$ will be reconstructed with the use of the TDSI algorithm. The equations of this algorithm for travel-time tomography of the atmosphere were derived in [11]. Here, it is shown how to apply TDSI to reciprocal transmission transducer arrays, when equation (1) can be split into two equations, equations (4) and (5). Application of TDSI to acoustic tomography with reciprocal sound transmission is similar to that for non-reciprocal sound propagation developed in [11–14]. Therefore, it is worthwhile presenting a brief overview of the main results obtained in these papers.

4.1. Time-dependent stochastic inversion

The starting equation for the reconstruction of the fluctuations $T(\mathbf{r}, t)$ and $\mathbf{V}(\mathbf{r}, t)$ is obtained from equation (1) where the first term is calculated with the use of the reconstructed values $\widehat{c}_0(t)$, $\widehat{u}_0(t)$ and $\widehat{v}_0(t)$. The remaining part can be written in the following form:

$$q_i(t) = q_{0i}(t) + \xi_i(t), \tag{16}$$

where

$$q_i(t) = L_i(\widehat{c}_0(t) - \mathbf{s}_i \cdot \widehat{\mathbf{V}}_0(t)) - \widehat{c}_0^2(t)t_i^{\mathrm{tr}}(t), \tag{17}$$

$q_{0i}(t)$ is noise-free data:

$$q_{0i}(t) = \int_{L_i}\left[\frac{\widehat{c}_0(t)}{2\widehat{T}_0(t)}T(\mathbf{r}, t) - \mathbf{s}_i \cdot \mathbf{V}(\mathbf{r}, t)\right]\mathrm{d}l, \tag{18}$$

and $\xi_i(t)$ represents noise in $q_i(t)$ due to the errors in travel time measurements, transducer position measurements and the reconstruction of mean fields.

Suppose that the travel times $\mathbf{t}^{\mathrm{tr}}(t) = \left[t_1^{\mathrm{tr}}(t); \ldots; t_I^{\mathrm{tr}}(t)\right]$ were measured at times $t_1, t_2, \ldots, t_Q$. For each t_k ($k = 1, 2, \ldots, Q$), the mean fields are estimated similarly to the technique described in section 3 (see also [11, 12, 14]), and vectors $\mathbf{q}(t_k)$ are formed. The key idea of TDSI is to use all Q vectors $\mathbf{q}(t_k)$ to reconstruct fluctuations $T(\mathbf{r}, t_0)$ and $\mathbf{V}(\mathbf{r}, t_0)$ at arbitrary time t_0.

Let $\mathbf{m}(t_0)$ be a vector of models which are subject to reconstruction:

$$\mathbf{m}(t_0) = [T(\mathbf{r}_1, t_0); \ldots; T(\mathbf{r}_J, t_0); u(\mathbf{r}_1, t_0); \ldots; u(\mathbf{r}_J, t_0); v(\mathbf{r}_1, t_0); \ldots; v(\mathbf{r}_J, t_0)], \tag{19}$$

where J is the total number of spatial points within a tomographic plane where the fluctuations should be reconstructed and $\mathbf{d}$ is a vector of data for this reconstruction:

$$\mathbf{d} = [\mathbf{q}(t_1); \mathbf{q}(t_2); \ldots; \mathbf{q}(t_Q)]. \tag{20}$$

Then, the optimal stochastic estimation $\widehat{\mathbf{m}}(t_0)$ of models $\mathbf{m}(t_0)$ is given by the following equation [11]:

$$\widehat{\mathbf{m}}(t_0) = \mathbf{R}_{\mathbf{md}}\mathbf{R}_{\mathbf{dd}}^{-1}\mathbf{d}, \tag{21}$$

where $\mathbf{R}_{\mathbf{md}} \equiv \langle \mathbf{m}\mathbf{d}^T \rangle$ and $\mathbf{R}_{\mathbf{dd}} \equiv \langle \mathbf{d}\mathbf{d}^T \rangle$ are model-data and data covariance matrices (the angular brackets $\langle\rangle$ denote the mathematical expectation). The estimation $\widehat{\mathbf{m}}(t_0)$ given by equation (21) minimizes the expected squared errors $\langle \epsilon_j^2 \rangle$ $(j = 1, \ldots, J)$ for each spatial point of the reconstruction [11, 15]: $\langle \epsilon_j^2 \rangle = \langle (m_j - \widehat{m}_j)^2 \rangle$.

The elements of $\mathbf{R}_{\mathbf{md}}$ and $\mathbf{R}_{\mathbf{dd}}$ matrices are calculated with the use of spatial–temporal covariance functions of temperature and wind-velocity fluctuations $B_{TT}(\mathbf{r}', t'; \mathbf{r}'', t'')$ and $B_{ij}(\mathbf{r}', t'; \mathbf{r}'', t'')$ (here, i and j indices indicate two components of wind-velocity fluctuations $\mathbf{V}(\mathbf{r}, t)$). Formulae for the calculation of the elements of noise-free matrices $\mathbf{R}_{\mathbf{md}_0}$ and $\mathbf{R}_{\mathbf{d}_0\mathbf{d}_0}$ are given by equations (18)–(21) from [11]. For convenience, these formulae are presented in appendix A. Matrices $\mathbf{R}_{\mathbf{md}}$ and $\mathbf{R}_{\mathbf{dd}}$ are obtained from $\mathbf{R}_{\mathbf{md}_0}$ and $\mathbf{R}_{\mathbf{d}_0\mathbf{d}_0}$ by taking into account noise in the input data, as shown in appendix A. To find analytical formulae for the spatial–temporal covariance functions $B_{TT}(\mathbf{r}', t'; \mathbf{r}'', t'')$ and $B_{ij}(\mathbf{r}', t'; \mathbf{r}'', t'')$, the hypothesis of frozen or locally frozen turbulence can be used [11–13, 28, 29]. These formulae can be found in appendix B.

The mean squared errors of $\widehat{\mathbf{m}}(t_0)$, which are the errors of the reconstruction of $\mathbf{m}(t_0)$, are given by the diagonal elements of the error covariance matrix $\mathbf{R}_{\epsilon\epsilon}$ [11]:

$$\mathbf{R}_{\epsilon\epsilon} = \mathbf{R}_{\mathbf{mm}} - \mathbf{R}_{\mathbf{md}}\mathbf{R}_{\mathbf{dd}}^{-1}\mathbf{R}_{\mathbf{md}}^T, \tag{22}$$

where $\mathbf{R}_{\mathbf{mm}} \equiv \langle \mathbf{m}(t_0)\mathbf{m}^T(t_0) \rangle$ is the model covariance matrix.

4.2. Error analysis in the data for TDSI

In this subsection, the covariance matrix of noise in the input data for TDSI, $\mathbf{R}_{\xi\xi}$, is calculated. Knowledge about noise in the input data is essential for TDSI since it appears in the $\mathbf{R}_{\mathbf{dd}}$ matrix, as shown in appendix A. The elements of the $\mathbf{R}_{\xi\xi}$ matrix are given by $\langle \xi_i(t)\xi_{i'}(t') \rangle$. To find these elements, one can take variations of equation (17) for different rays i and i' at different times t and t', multiply them, and take the mathematical expectation. Taking into account that for straight rays $L_i s_{ix} = (x_{Ri} - x_{Ti})$ and $L_i s_{iy} = (y_{Ri} - y_{Ti})$, where (x_{Ri}, y_{Ri}) and (x_{Ti}, y_{Ti}) are the coordinates of a receiver and a transmitter of the ith ray, correspondingly, one has:

$$\begin{aligned}\xi_i(t) = \delta q_i(t) = {} & L_i\delta\widehat{c}_0(t) + \widehat{c}_0(t)\delta L_i - \widehat{u}_0(t)(\delta x_{Ri} - \delta x_{Ti}) \\ & - \widehat{v}_0(t)(\delta y_{Ri} - \delta y_{Ti}) - (x_{Ri} - x_{Ti})\delta\widehat{u}_0(t) \\ & - (y_{Ri} - y_{Ti})\delta\widehat{v}_0(t) - \widehat{c}_0^2(t)\delta t_i^{\mathrm{tr}}(t) - 2\widehat{c}_0(t)t_i^{\mathrm{tr}}(t)\delta\widehat{c}_0(t).\end{aligned} \tag{23}$$

A similar equation can be written for a different path i' at a different time t'. Since $L_i^2 = (x_{Ri} - x_{Ti})^2 + (y_{Ri} - y_{Ti})^2$, then:

$$\begin{aligned}\delta L_i &= \frac{(x_{Ri} - x_{Ti})\,(\delta x_{Ri} - \delta x_{Ti}) + (y_{Ri} - y_{Ti})\,(\delta y_{Ri} - \delta y_{Ti})}{L_n} \\ &= s_{ix}(\delta x_{Ri} - \delta x_{Ti}) + s_{iy}(\delta y_{Ri} - \delta y_{Ti}).\end{aligned} \tag{24}$$

Taking into account that $\widehat{c}_0 t_i^{\mathrm{tr}} \sim L_i$, many of the cross-correlations equal zero, and neglecting the terms of order $(\widehat{V}_0/\widehat{c}_0)^2$, one has

$$\begin{aligned}\langle \xi_i(t)\xi_{i'}(t') \rangle \approx {} & 2\sigma_r^2\widehat{c}_0(t)\widehat{c}_0(t') - [\widehat{c}_0(t)\widehat{u}_0(t') + \widehat{c}_0(t')\widehat{u}_0(t)]s_{ix} \\ & - [\widehat{c}_0(t)\widehat{v}_0(t') + \widehat{c}_0(t')\widehat{v}_0(t)]s_{iy})\delta_{ii'} \\ & + L_i L_{i'}\big(\widehat{\sigma}_{c_0}^2 + s_{ix}s_{i'x}\widehat{\sigma}_{u_0}^2 + s_{iy}s_{i'y}\widehat{\sigma}_{v_0}^2\big)\delta_{tt'} + \widehat{c}_0^4(t)\sigma_t^2\delta_{ii'}\delta_{tt'},\end{aligned} \tag{25}$$

where σ_r^2 is the variance of the errors in transducer positions $\big(\sigma_r^2 = \langle(\delta x_{Ri})^2\rangle = \langle(\delta x_{Ti})^2\rangle = \langle(\delta y_{Ri})^2\rangle = \langle(\delta y_{Ti})^2\rangle\big)$, $\widehat{\sigma}_{c_0}^2$, $\widehat{\sigma}_{u_0}^2$, and $\widehat{\sigma}_{v_0}^2$ are variances of errors in the reconstruction of c_0, u_0, and v_0, correspondingly (see section 3 and similar formulae in [11, 12]), σ_t^2 is the variance of errors in the travel time measurements, and $\delta_{ii'}$ and $\delta_{tt'}$ are Kronecker's delta symbols. While deriving equation (25), it is assumed that uncertainties in the transducer positions are systematic in the sense that they do not change with time for any given path. As a result, the noise for the same paths is correlated for data measured at different times t and t' (the first term in equation (25)). Also, the errors in the reconstruction of mean fields at a given time t affect all data measured at this time (the second term in equation (25)). These two features result in the non-diagonal noise matrix $\mathbf{R}_{\xi\xi}$ which should be added to the noise-free data covariance matrix $\mathbf{R}_{\mathbf{d}_0\mathbf{d}_0}$ (see appendix A). Finally, in the particular case $t = t'$ and $i = i'$, equation (25) yields more accurate estimation of the variance $\sigma_{\xi_i}^2$ than that presented in [12].

4.3. TDSI for reciprocal arrays

The starting equations for the reconstruction of temperature and wind-velocity fluctuations are derived from equations (4) and (5):

$$q_{nT}(t) = q_{0nT}(t) + \xi_{nT}(t), \quad q_{nV}(t) = q_{0nV}(t) + \xi_{nV}(t), \tag{26}$$

where q_{nT} and q_{nV} are calculated with the use of the reconstructed mean values as described in section 3:

$$q_{nT}(t) = L_n\widehat{c}_0(t) - \widehat{c}_0^2(t)t_{nT}^{\mathrm{tr}}(t), \tag{27}$$

$$q_{nV}(t) = \widehat{c}_0^2(t)t_{nV}^{\mathrm{tr}}(t) - L_n(\widehat{u}_0 s_{nx} + \widehat{v}_0 s_{ny}), \tag{28}$$

the noise-free data q_{0nT} and q_{0nV} are given by the following expressions:

$$q_{0nT}(t) = \int_{L_n}\left[\frac{\widehat{c}_0(t)}{2\widehat{T}_0(t)}T(\mathbf{r}, t)\right]\mathrm{d}l, \tag{29}$$

$$q_{0nV}(t) = \int_{L_n}(u(\mathbf{r}, t)s_{nx} + v(\mathbf{r}, t)s_{ny})\,\mathrm{d}l, \tag{30}$$

and ξ_{nT} and ξ_{nV} represent the noise in the data due to the errors in measurements of travel times, positions of the transducers and reconstructions of the mean fields. The variances of these noises can be calculated similarly to the derivation shown in the previous subsection, but the analysis should be based on equations (27) and (28) instead of equation (17):

$$\begin{aligned}\langle \xi_{nT}(t)\xi_{n'T}(t') \rangle \approx {} & 2\sigma_r^2\widehat{c}_0(t)\widehat{c}_0(t')\delta_{nn'} \\ & + L_n L_{n'}\widehat{\sigma}_{c_0}^2\delta_{tt'} + \tfrac{1}{2}\widehat{c}_0^4(t)\sigma_t^2\delta_{nn'}\delta_{tt'},\end{aligned} \tag{31}$$

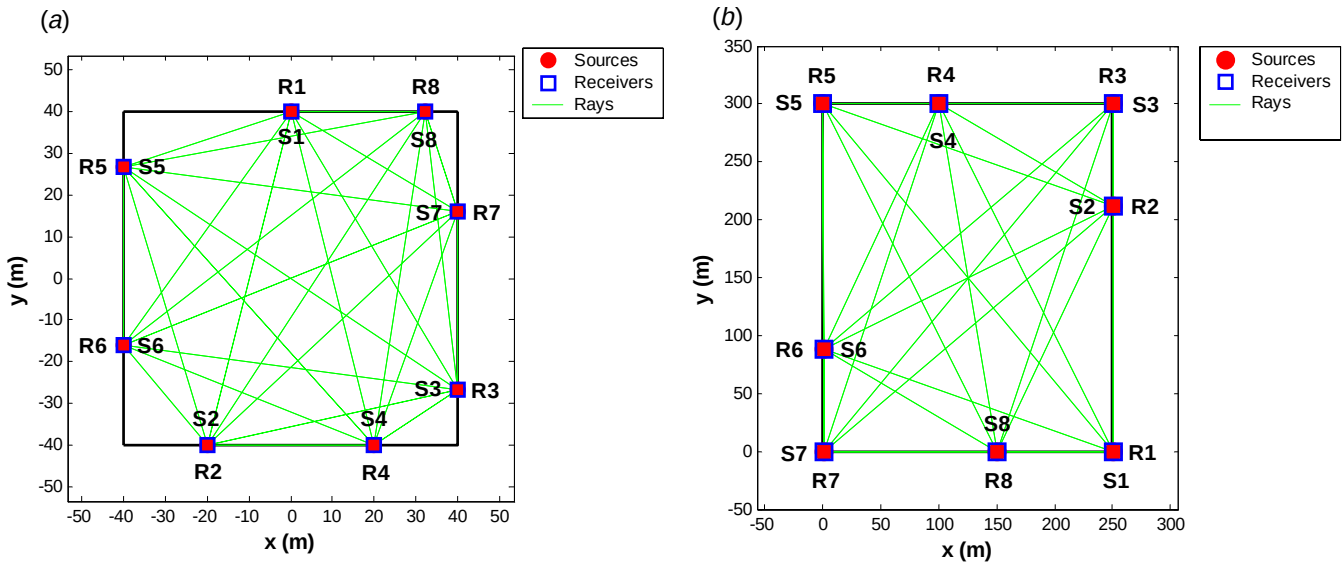

Figure 1. Tomographic arrays: (*a*) for the numerical experiment and (*b*) for the physical outdoor experiment.

$$\langle \xi_{nV}(t)\xi_{n'V}(t')\rangle \approx 2\sigma_r^2(\widehat{u}_0(t)\widehat{u}_0(t') + \widehat{v}_0(t)\widehat{v}_0(t'))\delta_{nn'} + L_n L_{n'} \times \left(s_{nx}s_{n'x}\widehat{\sigma}^2_{u_0} + s_{ny}s_{n'y}\widehat{\sigma}^2_{v_0}\right)\delta_{tt'} + \tfrac{1}{2}\widehat{c}_0^4(t)\sigma_t^2\delta_{nn'}\delta_{tt'}, \quad (32)$$

where indices n and n' denote two reciprocal paths. Note that the variance of t^{tr}_{nT} (the last term in equation (32)) is one-half of the variance of measured travel times. This is also true for t^{tr}_{nV}.

Comparing equation (18) with equations (29) and (30), one concludes that the general TDSI algorithm can be used for reconstruction of either the temperature or the wind-velocity fields with few modifications. For the temperature field T, one should use a different data vector $\mathbf{d}_T = [\mathbf{q}_T(t_1); \mathbf{q}_T(t_2); \ldots; \mathbf{q}_T(t_Q)]$, where $\mathbf{q}_T$ are given by equation (27), set the wind-velocity fluctuations to zero ($\sigma_V = 0$ in formulae (A.3) and (A.4) for the calculation of $\mathbf{R}_{\mathbf{md}_0}$ and $\mathbf{R}_{\mathbf{d}_0\mathbf{d}_0}$ matrices in appendix A) and use equation (31) instead of equation (25) to calculate the error matrix, which is needed in order to find the matrix $\mathbf{R}_{\mathbf{dd}}$. Correspondingly, to reconstruct the field of wind-velocity fluctuations$\mathbf{V}$, one should use the data vector $\mathbf{d}_V = [\mathbf{q}_V(t_1); \mathbf{q}_V(t_2); \ldots; \mathbf{q}_V(t_Q)]$, where $\mathbf{q}_V$ are given by equation (28), set $\sigma_T = 0$ in formulae (A.3) and (A.4), and use equation (32) to calculate the noise.

5. Numerical experiment

In this section, a numerical two-dimensional tomography experiment is described. The primary goal of this numerical experiment is to study whether the analytical separation of travel times in reciprocal transmission arrays, given by equations (4) and (5), improves the reconstruction in comparison with the general TDSI algorithm based on equation (1). The secondary goal is to compare the reconstruction quality of TDSI and ordinary SI algorithms on non-frozen turbulence.

For these purposes, the original temperature and wind-velocity LES fields were used. The particular simulation analyzed here involves unstable atmospheric stratification. Five time frames ($Q = 5$) of two-dimensional temperature and wind-velocity fields were employed with a time interval of 4.6 s at height $z = 13.75$ m. The spatial resolution of LES was 4 m in the horizontal plane. More detailed information about LES fields used in the numerical experiment described can be found in [38]. Using these LES fields, the travel times were calculated for each time frame in accordance with equation (1) for the reciprocal transmission array shown in figure 1(*a*). The array consisted of eight sound sources (S1, . . . , S8) and eight receivers (R1, . . . , R8) arranged along the perimeter of a square with an 80 m length side. (Note that a similar array is currently under construction at the National Oceanic and Atmospheric Administration, Boulder, CO.) The array provided 56 travel times (eight sources × eight receivers − eight paths of zero length) for each time frame (28 reciprocal travel paths). To take into account the noise in travel-time measurements, the normally distributed white noise with $\sigma_t = 5$ μs was added to the calculated travel times (for each path at each time frame). This magnitude of noise corresponds to 3% of errors in the data for the reconstruction of fluctuations (see equation (16)). Moreover, during the calculations of travel times, the transducer positions were randomly distorted by normally distributed white noise with $\sigma_r = 0.01$ m to represent the uncertainty in the transducer positions. These random deviations from the original locations remained the same for all five time frames to imitate the systematic errors. The objective of the experiment was to reconstruct the temperature and wind-velocity fields at the third time frame ($t_0 = 3$).

The reconstruction of mean fields has been implemented for the separated travel times as described in section 3, and the reconstruction based on the travel times without separation is described in [11–13]. The true and reconstructed mean fields are presented in table 1, where 'modified alg.' and 'general alg.' refer to the reconstruction with and without travel-time separation, correspondingly. According to table 1, the values of the mean fields reconstructed by both modified and general algorithms are the same. The only difference is

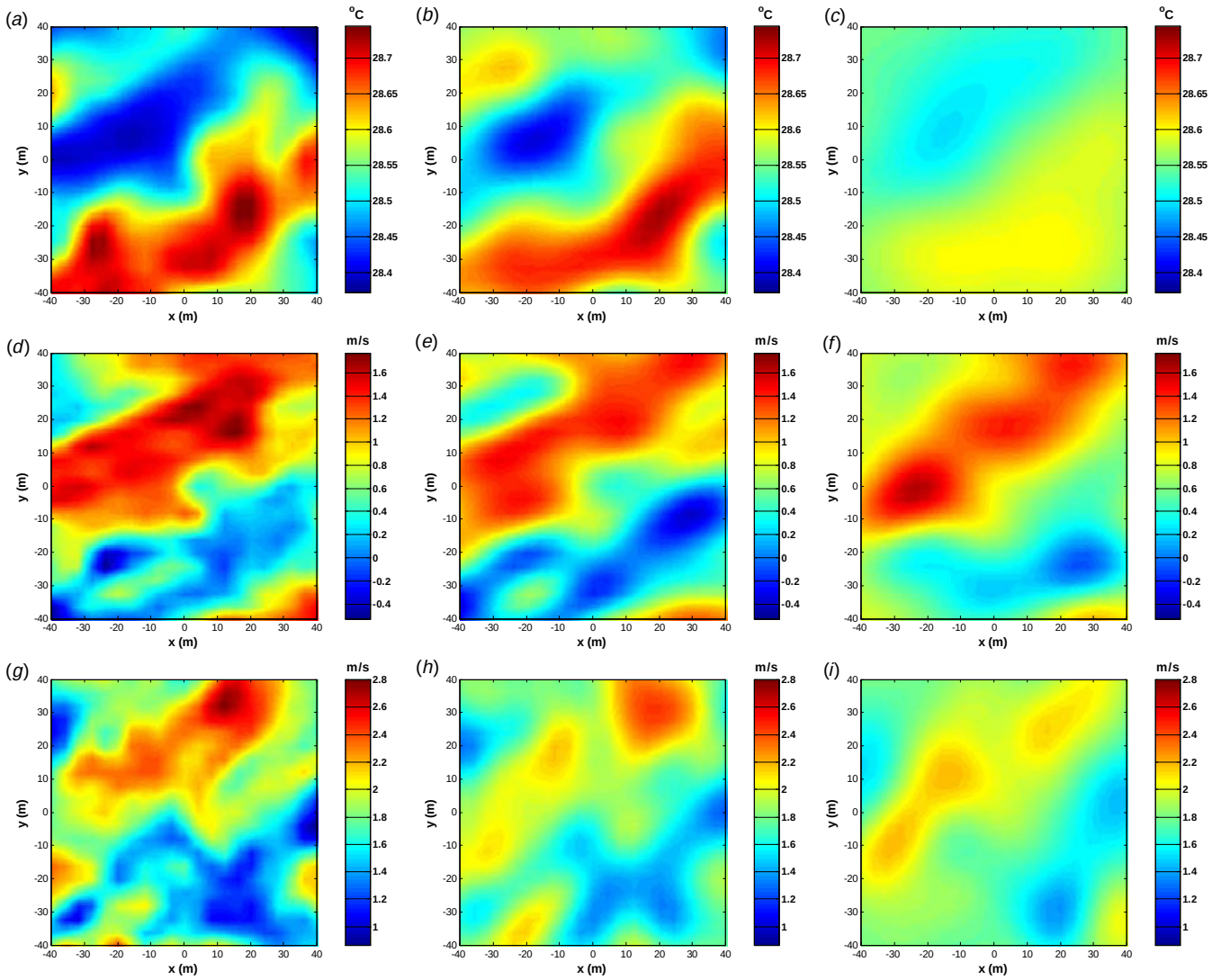

Figure 2. Original LES and reconstructed temperature and wind-velocity fields at frame 3 in the numerical experiment. (*a*), (*d*) and (*g*): original fields of temperature and two components of wind velocity. (*b*), (*e*) and (*h*): fields reconstructed by TDSI. (*c*), (*f*) and (*i*): fields reconstructed by SI.

Table 1. Actual and reconstructed mean temperature and wind-velocity fields.

Fields	T_0 (°C)	u_0 (m s^{-1})	v_0 (m s^{-1})
True	28.55	0.80	1.82
General alg.	28.56 ± 0.07	0.80 ± 0.05	1.82 ± 0.05
Modified alg.	28.56 ± 0.01	0.80 ± 0.08	1.82 ± 0.08

in the estimated errors of the reconstruction. But these errors are still of the same order. Another conclusion from table 1 is that the reconstruction of the mean fields is very accurate. Comparing the true and reconstructed values, one can see that the actual discrepancy is of order 0.01 °C for temperature and less than 0.01 m s^{-1} for wind velocity.

The reconstruction of the fluctuations was implemented by TDSI and SI algorithms with and without analytical separation of travel times. For the TDSI, the data from all five time frames were used to reconstruct the fields at time t_0, while SI utilizes the data measured at the same time frame t_0. The variances and correlation lengths of turbulence for stochastic inversion algorithms were estimated from the original LES fields: $\sigma_T = 0.08$ °C, $\sigma_V = 0.38$ m s^{-1} and $l_T = l_V = 14$ m. Figure 2 shows the original and full fields $\widetilde{T}$, $\widetilde{u}$, and $\widetilde{v}$ reconstructed without travel-time separation. The original LES fields are presented in figures 2(*a*), (*d*) and (*g*). The fields reconstructed by the TDSI algorithm are shown in figures 2(*b*), (*e*) and (*h*). The reconstruction with the use of SI is presented in figures 2(*c*), (*f*) and (*i*). Comparing these figures, one notes a remarkable improvement in the reconstruction done by TDSI in comparison with that done by SI. In the case of SI, the temperature field is reconstructed rather poorly. Neither the shape of turbulent eddies nor their magnitude is reconstructed sufficiently well (see figure 2(*c*)). In contrast, the TDSI algorithm (figure 2(*b*)) captures both the shape and the magnitude even though the smallest details are still omitted. The SI algorithm reconstructs the wind-velocity components better than the temperature field (see figures 2(*f*) and (*i*)), but still not as well as the TDSI algorithm (figures 2(*e*) and (*h*)). For example, the shape of blue eddies in the u and v fields is

Table 2. Actual and expected RMSE of the reconstruction by TDSI and SI algorithms.

	RMSE	$\widetilde{T}$ (°C)	$\widetilde{u}$ (m s^{-1})	$\widetilde{v}$ (m s^{-1})
TDSI	General algorithm			
	Actual	0.05	0.233	0.215
	Expected	0.08	0.235	0.208
	Modified algorithm			
	Actual	0.05	0.226	0.209
	Expected	0.05	0.233	0.207
SI	General algorithm			
	Actual	0.07	0.313	0.286
	Expected	0.10	0.330	0.267
	Modified algorithm			
	Actual	0.08	0.307	0.284
	Expected	0.08	0.326	0.266

not reconstructed correctly by SI while TDSI reconstructs it rather well.

These observations are summarized in table 2, which represents actual and expected root mean squared errors (RMSE) for the general (without the separation of travel times) and modified (with travel times being separated) algorithms for the case of SI and TDSI. The actual RMSE is calculated with the use of an actual discrepancy between the original and reconstructed fields. The expected spatially averaged RMSE of the full fields are calculated with the use of equations (8) and (14) for the mean fields and equation (22) for the fluctuations. Comparing the actual errors of the general and modified algorithms (lines 1 and 3 for TDSI and lines 5 and 7 for SI in table 2), one concludes that these algorithms yield almost identical results. This means that the analytical separation of the travel times does not improve the reconstruction quality of the stochastic inversion algorithms. On the other hand, if one compares the actual errors of TDSI and SI reconstructions (lines 1 and 5 for the general algorithm and lines 3 and 7 for the modified one), then it is noticeable that TDSI always outperforms SI. This is clearly seen in figure 2 as well. Finally, the comparison of the actual and expected errors for the same algorithms reveals that the technique used for the error estimation yields accurate and reliable results.

It is interesting to point out that the 'invisible' wind-velocity fields, which are mentioned in section 2 and [34, 35], did not introduce significant errors in the reconstruction. The actual RMSE are small and in a good agreement with the expected RMSE. Two explanations are plausible. First, these 'invisible' fields were not reconstructed but they were much weaker than 'visible' ones, which were reconstructed from travel times, so that they could not distort the reconstructed fields significantly (within the actual RMSE of reconstruction). This point can be supported by the following reasoning. The use of Taylor's or locally frozen turbulence hypotheses in TDSI may be viewed as effective moving the transducer array through motionless turbulence. This is equivalent to having some transducers not only along the borders of the tomographic area but also inside. The data obtained from such an extended transducer array at several time frames may reveal 'invisible' fields that exist longer than the time interval between the frames. Since the time interval between two consecutive measurements can be quite small (it is an adjustable parameter in experiments), only really short-time and weak 'invisible' fields may remain unrevealed. Second, the 'invisible' fields may be reconstructed by stochastic inversion algorithms (in full or partially). As shown in section 4, these algorithms incorporate additional statistical information about true fields. This information supplements the travel-time measurements (in analogy to the additional measurements proposed in [34]). Then, the 'invisible' fields are reconstructed by stochastic inversion algorithms as a complement to the 'visible' fields so that the total fields would have specific correlation properties.

Table 3. Mean temperature and wind-velocity fields reconstructed in the outdoor experiment.

Fields	T_0 (°C)	u_0 (m s^{-1})	v_0 (m s^{-1})
General alg.	27.30 ± 0.06	-0.15 ± 0.05	0.27 ± 0.05
Modified alg.	27.30 ± 0.07	-0.15 ± 0.05	0.27 ± 0.05

Table 4. Expected RMSE of the reconstruction by TDSI algorithm in the outdoor experiment.

RMSE	$\widetilde{T}$ (°C)	$\widetilde{u}$ (m s^{-1})	$\widetilde{v}$ (m s^{-1})
General alg.	0.08	0.26	0.25
Modified alg.	0.09	0.26	0.25

6. Physical outdoor experiment

This section describes a physical outdoor experiment with a reciprocal transmission array carried out as a part of the experiment STructure of turbulent transport under INHOmogeneous surface conditions (STINHO) on June 17, 2002, in Lindenberg, Germany [7]. The array consisted of eight sound sources and eight sound receivers arranged along the perimeter of 250 m $\times$ 300 m as shown in figure 1(*b*). The travel times were measured each minute. The order of errors in the measurements was $\sigma_t = 0.1$ ms for the travel times and $\sigma_r = 0.01$ m for the transducer positions. The fields at 1753 UTC (universal time coordinated) were the subject of reconstruction.

The reconstruction was implemented in the same manner as it was for the numerical experiment except that there were no true fields and actual errors of the reconstruction. However, the results of the numerical experiment suggest that the reconstruction by TDSI is quite accurate, and the expected errors yield an accurate estimation of the actual ones.

The reconstruction of mean fields by general and modified algorithms is presented in table 3. Similar to the numerical experiment, the reconstructed values and expected RMSE are the same for the general and modified algorithms. As one can see, the expected RMSE are 0.06 °C for temperature and 0.05 m s^{-1} for wind velocity. This accuracy is sufficient for most meteorological applications.

For the TDSI algorithm, the variance of temperature fluctuations was estimated with the use of an *in situ* sensor located within a tomographic plane: $\sigma_T = 0.06$ °C. The variance of the wind-velocity fluctuations was not measured

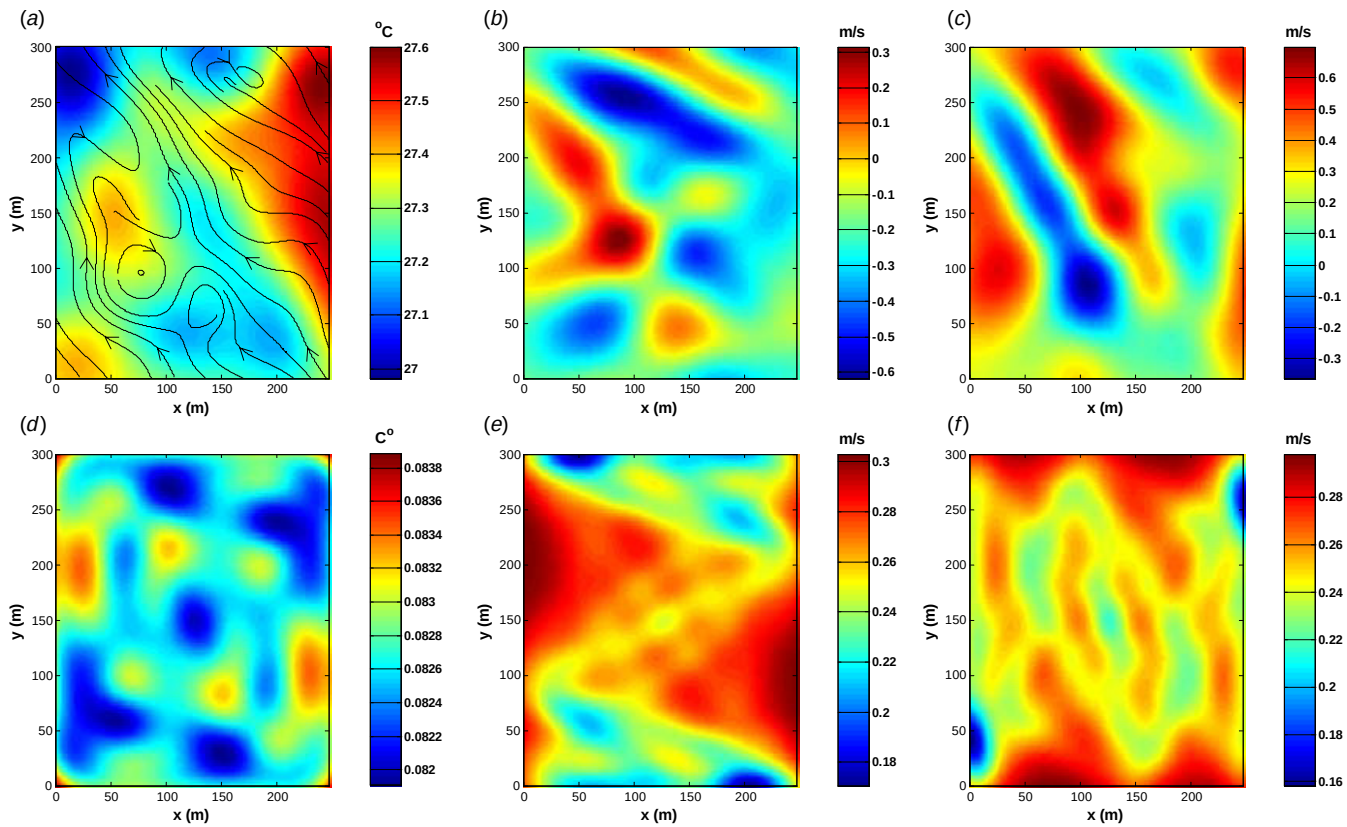

Figure 3. Physical outdoor experiment. (*a*)–(*c*): temperature and two components of wind-velocity fields reconstructed by TDSI. The black lines in (*a*) indicate the reconstructed wind. (*d*)–(*f*): the expected errors of the reconstruction shown in (*a*)–(*c*), correspondingly.

in this experiment but was measured in similar outdoor experiments [7, 12]. In the experiment described, the typical value $\sigma_V = 0.3$ m s^{-1} had been used. The correlation lengths of the fluctuations, which define a desirable characteristic size of the reconstructed turbulent eddies, were $l_T = l_V = 40$ m. The travel times from three consecutive frames were used (1752, 1753 and 1754 UTC) to reconstruct the fluctuations at 1753 UTC. The reconstructed full fields (the mean fields plus the fluctuations) are presented in figures 3(*a*)–(*c*). The black lines in figure 3(*a*) represent the reconstructed wind. The expected RMSE of the reconstruction are shown in figures 3(*d*)–(*f*). Note that the errors are smaller than the range of the fluctuations, which means that the temperature and wind-velocity eddies which are seen in figures 3(*a*)–(*c*) are reconstructed reliably.

7. Summary and conclusions

The main goal of this paper was to study whether reciprocal transmission arrays improve tomographic reconstruction of atmospheric temperature and wind-velocity fields when implemented by stochastic inversion algorithms. It is known that, for the linearized problem, reciprocal transmission arrays allow one to separate the measured travel times into two components, one of which depends on the temperature field only while another depends on the wind-velocity field. Also, it is well known that such an approach improves the reconstructions by some other algorithms since it increases the data/unknowns ratio. However, application of this technique to stochastic inversion algorithms has not been studied. The results obtained in this paper suggest that the modified and general stochastic inversion algorithms (with and without analytical separation of travel times, correspondingly) yield practically identical reconstructions. This conclusion has been verified for the TDSI and SI algorithms on the numerical and real experimental data.

Another new contribution of this paper is an improved model of noise in the data for reconstruction of the fluctuations with the use of SI and TDSI. The present formulation, unlike previous ones, accounts for systematic noise in the transducer positions, which better corresponds to a real experiment. As a result, the covariance matrix of noise is no longer diagonal. This extension provides more accurate reconstruction (and estimation of the errors in reconstruction) than previously.

Finally, the TDSI algorithm has been tested for the first time on the original LES fields which were not frozen. The TDSI algorithm accounts for the correlation of the temperature and wind-velocity fields not only in space but also in time. To find the spatial–temporal covariance functions of the fluctuations, a hypothesis of locally frozen turbulence was utilized. Since this hypothesis makes certain assumptions about turbulence which may not occur in real turbulence, the TDSI algorithm might not result in a better reconstruction than the ordinary SI algorithm, which is free from these assumptions. The numerical results obtained in this paper (figure 2 and table 2) show that the TDSI reconstruction, which

utilizes the locally frozen turbulence hypothesis [12, 28] based on Gaussian spatial covariance functions, is remarkably better than the SI reconstruction despite the facts that the LES fields being reconstructed did not actually have a Gaussian spatial covariance and may not exactly satisfy the assumptions of this hypothesis.

Acknowledgments

This research is partly based upon work that was supported by the US Army Research Office under contract number W911NF-06-1-0007 and by the German Research Foundation (Deutsche Forschungsgemeinschaft), grant numbers ZI 623/3-2 and Ra 569/9-1. LES data were provided by E G Patton and P P Sullivan from the National Center for Atmospheric Research. The LES was supported in part by the DoD High-Performance Computing Modernization Program. The data for the outdoor experiment were provided by K Arnold from University of Leipzig, Germany.

Appendix A. Elements of matrices $\mathbf{R_{md}}$ and $\mathbf{R_{dd}}$

In this appendix, formulae for $\mathbf{R_{dd}}$ and $\mathbf{R_{md}}$ matrices are presented.

The data vector $\mathbf{d}$, given by equation (20), contains noise due to errors in the travel-time measurements, transducer positions and the reconstructed mean fields. Therefore, the data vector $\mathbf{d}$ can be presented as $\mathbf{d} = \mathbf{d}_0 + \Delta\mathbf{d}$, where $\mathbf{d}_0 = [\mathbf{q}_0(t_1); \mathbf{q}_0(t_2); \ldots; \mathbf{q}_0(t_Q)]$ is a noise-free data vector, whose elements are given by equation (18), and $\Delta\mathbf{d} = [\boldsymbol{\xi}(t_1); \boldsymbol{\xi}(t_2); \ldots; \boldsymbol{\xi}(t_Q)]$ is a vector of uncertainties with zero mathematical expectation: $\langle\Delta\mathbf{d}\rangle = \mathbf{0}$. Assuming that $\Delta\mathbf{d}$ is independent of $\mathbf{m}$ and $\mathbf{d}_0$, one has

$$\mathbf{R_{md}} = \langle\mathbf{m}\mathbf{d}^T\rangle = \left\langle\mathbf{m}\mathbf{d}_0^T\right\rangle + \langle\mathbf{m}\rangle\langle\Delta\mathbf{d}^T\rangle = \left\langle\mathbf{m}\mathbf{d}_0^T\right\rangle, \tag{A.1}$$

$$\mathbf{R_{dd}} = \langle\mathbf{d}\mathbf{d}^T\rangle = \left\langle\mathbf{d}_0\mathbf{d}_0^T\right\rangle + \langle\Delta\mathbf{d}\Delta\mathbf{d}^T\rangle. \tag{A.2}$$

As one can see, noise in the data does not affect the model-data noise-free covariance matrix ($\mathbf{R_{md_0}} = \mathbf{R_{md}}$) but changes the data-data noise-free matrix $\mathbf{R_{d_0d_0}}$. Namely, one should know the noise covariance matrix $\mathbf{R}_{\xi\xi} = \langle\Delta\mathbf{d}\Delta\mathbf{d}^T\rangle$. The elements of this matrix are calculated in section 4.2.

To calculate the elements of noise-free matrices $\left\langle\mathbf{m}\mathbf{d}_0^T\right\rangle$ and $\left\langle\mathbf{d}_0\mathbf{d}_0^T\right\rangle$ in equations (A.1) and (A.2), one should take into account equation (18):

$$\begin{aligned}\langle m_j(t_0)q_{0i}(t_k)\rangle &= \int_{L_i} \mathrm{d}l \left\{ \frac{\widehat{c}_0(t_k)}{2\widehat{T}_0(t_k)} \langle m_j(t_0)T(\mathbf{r},t_k)\rangle \right.\\ &\left. + \langle m_j(t_0)u(\mathbf{r},t_k)\rangle s_{ix} + \langle m_j(t_0)v(\mathbf{r},t_k)\rangle s_{iy} \right\}\\ &= \begin{cases} \int_{L_i} \mathrm{d}l \left[\frac{\widehat{c}_0(t_k)}{2\widehat{T}_0(t_k)} B_{TT}(\mathbf{r}_j,t_0;\mathbf{r},t_k) \right], & \text{if } 1 \leqslant j \leqslant J,\\ \int_{L_i} \mathrm{d}l [B_{uu}(\mathbf{r}_{j-J},t_0;\mathbf{r},t_k)s_{ix} + B_{uv}(\mathbf{r}_{j-J},t_0;\mathbf{r},t_k)s_{iy}], & \\ \qquad \text{if} \quad J+1 \leqslant j \leqslant 2J, & \\ \int_{L_i} \mathrm{d}l [B_{vu}(\mathbf{r}_{j-2J},t_0;\mathbf{r},t_k)s_{ix} + B_{vv}(\mathbf{r}_{j-2J},t_0;\mathbf{r},t_k)s_{iy}], & \\ \qquad \text{if} \quad 2J+1 \leqslant j \leqslant 3J, & \end{cases}\end{aligned} \tag{A.3}$$

where $i = 1, 2, \ldots, I$, $j = 1, 2, \ldots, 3J$, $k = 1, 2, \ldots, Q$, $\mathbf{r} \in L_i$, B_{TT}, B_{uu}, B_{vv} and B_{uv} are the spatial–temporal covariance functions of the corresponding fields labeled by the subscripts, and the $\mathbf{r}_j$ are the spatial points within the tomographic plane at which the fields are being reconstructed; these points remain fixed during the integration.

Similarly, an expression for the covariance matrix $\left\langle\mathbf{d}_0\mathbf{d}_0^T\right\rangle$ between the noise-free data at time t_n and time t_k can be calculated:

$$\begin{aligned}\langle q_{0i}(t_n)q_{0p}(t_k)\rangle = \int_{L_i} \mathrm{d}l \int_{L_p} \mathrm{d}l' \left\{ \frac{\widehat{c}_0(t_k)\widehat{c}_0(t_n)}{4\widehat{T}_0(t_k)\widehat{T}_0(t_n)} B_{TT}(\mathbf{r},t_n;\mathbf{r}',t_k) \right.\\ + B_{uu}(\mathbf{r},t_n;\mathbf{r}',t_k)s_{ix}s_{px} + B_{vv}(\mathbf{r},t_n;\mathbf{r}',t_k)s_{iy}s_{py}\\ \left. + B_{uv}(\mathbf{r},t_n;\mathbf{r}',t_k)s_{ix}s_{py} + B_{vu}(\mathbf{r},t_n;\mathbf{r}',t_k)s_{iy}s_{px} \right\},\end{aligned} \tag{A.4}$$

where $i, p = 1, 2, \ldots, I, n, k = 1, 2, \ldots, Q, \mathbf{r} \in L_i$, and $\mathbf{r}' \in L_p$. Note that $B_{vu}(\mathbf{r},t_1;\mathbf{r}',t_2) = B_{uv}(\mathbf{r}',t_2;\mathbf{r},t_1)$, and similarly for other fields. When deriving equations (A.3) and (A.4), it is assumed that $B_{Tu} = B_{Tv} \equiv 0$.

Appendix B. Spatial–temporal covariance functions

In this appendix, analytical formulae for spatial–temporal covariance functions of temperature and wind-velocity fluctuations are presented. These formulae were derived with the use of the locally frozen turbulence hypothesis [12, 28] which is a generalization of the widely used rigidly frozen turbulence hypothesis (Taylor's hypothesis). In the latter it is assumed that each point of a turbulent eddy is advected with a constant velocity. As a result, the eddy remains 'frozen' as it moves. In contrast, in the locally frozen turbulence hypothesis, it is assumed that each point of the eddy can move with its own velocity. Therefore, the turbulence is no longer 'frozen' since turbulent eddies can arbitrarily change their shape. If the wind velocity was constant, the locally frozen turbulence hypothesis coincides with Taylor's hypothesis.

For the two-dimensional case, the formulae for the spatial–temporal covariance functions of temperature and wind-velocity fluctuations at points $\mathbf{r}'$ and $\mathbf{r}''$ and times t' and t'' take the following form [12]:

$$B_{TT}(\boldsymbol{\rho},\tau) = \tilde{\sigma}_T^2 \exp\left[-\frac{(\boldsymbol{\rho} - \mathbf{V}_0(t')\tau)^2}{\tilde{l}_T^2} \right], \tag{B.1}$$

$$\begin{aligned}B_{uu}(\boldsymbol{\rho},\tau) &= \tilde{\sigma}_V^2 \exp\left[-\frac{(\boldsymbol{\rho} - \mathbf{V}_0(t')\tau)^2}{\tilde{l}_V^2} \right]\\ &\times \left(1 - \frac{(\rho_y - v_0(t')\tau)^2}{\tilde{l}_V^2} \right),\end{aligned} \tag{B.2}$$

$$\begin{aligned}B_{uv}(\boldsymbol{\rho},\tau) &= \tilde{\sigma}_V^2 \exp\left[-\frac{(\boldsymbol{\rho} - \mathbf{V}_0(t')\tau)^2}{\tilde{l}_V^2} \right]\\ &\times \frac{(\rho_x - u_0(t')\tau)(\rho_y - v_0(t')\tau)}{\tilde{l}_V^2},\end{aligned} \tag{B.3}$$

where $\boldsymbol{\rho} = \mathbf{r}'' - \mathbf{r}'$, $\tau = t'' - t'$, $\mathbf{V}_0$ is a spatially averaged wind velocity with components (u_0, v_0), and the effective variances

$\tilde{\sigma}_T^2$ and $\tilde{\sigma}_V^2$, and the squares of correlation lengths $\tilde{l}_T^2$ and $\tilde{l}_V^2$ are given by

$$\tilde{\sigma}_T^2 = \frac{\sigma_T^2}{\left[1 + 2\left(\frac{\sigma_V \tau}{l_T}\right)^2\right]^{3/2}}, \qquad \tilde{l}_T^2 = l_T^2 + 2\sigma_V^2 \tau^2, \tag{B.4}$$

$$\tilde{\sigma}_V^2 = \frac{\sigma_V^2}{\left[1 + 2\left(\frac{\sigma_V \tau}{l_V}\right)^2\right]^{3/2}}, \qquad \tilde{l}_V^2 = l_V^2 + 2\sigma_V^2 \tau^2. \tag{B.5}$$

Here, σ_T, σ_V, l_T and l_V are variances and correlation lengths of the fluctuations at the same time ($\tau = 0$). Formulae for B_{uv} and B_{vv} are symmetric to those given by equations (B.2) and (B.3). Note that the space variations of the full wind velocity field $\tilde{\mathbf{V}}(\mathbf{r}, t)$ in the locally frozen turbulence hypothesis are reflected in formulae (B.1)–(B.5) through σ_V.

In the limiting case $\sigma_V \tau / \min\{l_V, l_T\} \to 0$ and time-independent $\mathbf{V}_0$, these formulae yield the results for rigidly frozen turbulence [11]. It follows from equations (B.1)–(B.5) that the dependence of the spatial–temporal covariance functions on τ in the locally frozen turbulence hypothesis is manifested in three effects: the spatial arguments of the covariance functions are shifted by the vector $\mathbf{V}_0(t')\tau$, the effective variances of the fluctuations $\tilde{\sigma}_T^2$ and $\tilde{\sigma}_V^2$ decrease, and the effective correlation lengths $\tilde{l}_T$ and $\tilde{l}_V$ increase as τ increases.

References

[1] Wilson D K and Thomson D W 1994 Acoustic tomographic monitoring of the atmospheric surface layer *J. Atmos. Ocean. Technol.* **11** 751–69

[2] Ziemann A, Arnold K and Raabe A 1999 Acoustic tomography in the atmospheric surface layer *Ann. Geophys.* **17** 139–48

[3] Arnold K, Ziemann A and Raabe A 2001 Tomographic monitoring of wind and temperature at different heights above the ground *Acust., Acta Acust.* **87** 703–8

[4] Wilson D K, Ziemann A, Ostashev V E and Voronovich A G 2001 An overview of acoustic travel-time tomography in the atmosphere and its potential applications *Acust., Acta Acust.* **87** 721–30

[5] Vecherin S N, Ostashev V E, Wilson D K, Voronovich A G, Goedecke G H, Collier S L, Noble J M and Ligon D 2004 Forward and inverse problems of acoustic tomography of the atmosphere *Proc. 11th Int. Symp. on Long Range Sound Propagation (Fairlee, VT)*

[6] Holstein P, Raabe A, Müller R, Barth M, Mackenzie D and Starke E 2004 Acoustic tomography on the basis of travel-time measurement *Meas. Sci. Technol.* **15** 1420–8

[7] Raabe A *et al* 2005 STINHO-STructure of turbulent transport under INHOmogeneous surface conditions—a micro-α scale field experiment and LES modelling *Meteorol. Z.* **14** 315–27

[8] Bender M and Raabe A 2007 Preconditions to ground based GPS water vapour tomography *Ann. Geophys.* **25** 1727–34

[9] Kunitsyn V E and Tereshchenko E D 2003 *Ionospheric Tomography* (Berlin: Springer)

[10] Gan T H, Hutchins D A, Carpenter P W and Wright W M D 2003 Simultaneous reconstruction of flow and temperature cross-sections in gases using acoustic tomography *J. Acoust. Soc. Am.* **114** 759–66

[11] Vecherin S N, Ostashev V E, Goedecke G H, Wilson D K and Voronovich A G 2006 Time-dependent stochastic inversion in acoustic travel-time tomography of the atmosphere *J. Acoust. Soc. Am.* **119** 2579–88

[12] Vecherin S N, Ostashev V E, Ziemann A, Wilson D K, Arnold K and Barth M 2007 Tomographic reconstruction of atmospheric turbulence with the use of time-dependent stochastic inversion *J. Acoust. Soc. Am.* **122** 1416–25

[13] Vecherin S N 2007 Acoustic travel-time tomography of the atmosphere *Doctoral Dissertation* New Mexico State University, Las Cruces, NM

[14] Vecherin S N, Ostashev V E and Wilson D K 2008 Three-dimensional acoustic travel-time tomography of the atmosphere *Acust., Acta Acust.* **94** 349–58

[15] Aki K and Richards P G 1980 *Quantitative Seismology. Theory and Methods* (San Francisco: Freeman)

[16] Bretherton F P, Davis R E and Fandry C B 1976 A technique for objective analysis and design of oceanographic experiments applied to MODE-73 *Deep-Sea Res.* **23** 559–82

[17] Gilson J, Roemmich D, Cornuelle B D and Fu L-L 1998 Relationship of TOPEX/Poseidon altimetric height to steric height and circulation in the North Pacific *J. Geophys. Res.* **103** 965

[18] Ducet N, Le Traon P Y and Reverdin G 2000 Global high-resolution mapping of ocean circulation from TOPEX/Poseidon and ERS-1 and -2 *J. Geophys. Res.* **105** 498

[19] Galatsanos N P and Chin R T 1989 Digital restoration of multichannel images *IEEE Trans. Acoust. Speech Signal Process.* **37** 415–21

[20] Ozkan M K, Erdem A T, Sezan M I and Tekalp A M 1992 Efficent multiframe Wiener restoration of blurred and noisy image sequences *IEEE Trans. Image Process.* **1** 453–76

[21] Links J M, Prince J L and Gupta S N 1996 A vector Wiener filter for dual-radionuclide imaging *IEEE Trans. Med. Imaging* **15** 700–9

[22] Kalman R E 1960 A new approach to linear filtering and prediction problems *Trans. ASME* D **82** 35–45

[23] Brown R G and Hwang Y C 1992 *Introduction to Random Signals and Applied Kalman Filtering* 2nd edn (New York: Wiley)

[24] Artemiev V M, Naumov A O and Tillack G-R 2001 Recursive tomographic image reconstruction using a Kalman filter approach in the time domain *J. Phys. D: Appl. Phys.* **34** 2073–83

[25] Lee T H, Ra W-S, Yoon T S and Park J B 2004 Robust Kalman filtering via Krein space estimation *IEE Proc.* **151** 59–63

[26] Shinke T, Yoshikawa Y, Kamoshida T and Mitsudera H 2001 Analysis method for ocean acoustic tomography data using Kalman filter: evaluation by identical twin experiment *Japan. J. Appl. Phys.* **40** 3835–41

[27] Trigo F C, Gonzalez-Lima R and Amato M B P 2004 Electrical impedance tomography using the extended Kalman filter *IEEE Trans. Biomed. Eng.* **51** 72–81

[28] Tatarskii V I 1971 *The Effects of the Turbulent Atmosphere on Wave Propagation* (Jerusalem: Keter)

[29] Hinze J 1975 *Turbulence* 2nd edn (New York: McGraw-Hill)

[30] Kaimal J C and Finnigan J J 1994 *Atmospheric Boundary Layer Flows: Their Structure and Measurement* (New York: Oxford University Press)

[31] Ostashev V E 1997 *Acoustics in Moving Inhomogeneous Media* (London: E&FN Spon)

[32] Wilson D K, Brasseur J G and Gilbert K E 1999 Acoustic scattering and the spectrum of atmospheric turbulence *J. Acoust. Soc. Am.* **105** 30–4

[33] Johnson S A, Greenleaf J F, Hansen C R, Samayoa W F, Tanaka M, Lent A, Christensen D A and Woolley R L 1977 Reconstructing three-dimensional fluid velocity vector fields from acoustic transmission measurements *Acoustical Holography* vol 7, ed L W Kessler (New York: Plenum) pp 307–26

[34] Braun H and Hauck A 1991 Tomographic reconstruction of vector fields *IEEE Trans. Signal Process.* **39** 464–71

[35] Norton S J 1992 Unique tomographic reconstruction of vector fields using boundary data *IEEE Trans. Image Process.* **1** 406–12

[36] Munk W H, Worcester P and Wunsch C 1995 *Ocean Acoustic Tomography* (New York: Cambridge University Press)

[37] Barth M, Raabe A, Arnold K, Resagk C and Puits R Du 2007 Flow field detection using acoustic travel-time tomography *Meteorol. Z.* **16** 443–50

[38] Sullivan P P, McWilliams J C and Moeng C H 1994 A subgrid-scale model for large-eddy simulation of planetary boundary layer flows *Bound.-Layer Meteorol.* **71** 247–76

[39] Campbell S L and Meyer C D Jr 1991 *Generalized Inverses of Linear Transformations* (New York: Dover)